IMPLEMENTATION OF A TIME OF FLIGHT DETECTION SYSTEM FOR ELASTICALLY RECOILED IONS AT THE ITHEMBA LABORATORY FOR ACCELERATOR BASED SCIENCES (ITHEMBA LABS)

by

Stephen Sepuru

A dissertation submitted in partial fulfillment of the requirements for the degree of

Master of Science in Applied Radiation Science and Technology

in the

Faculty of Agriculture, Science and Technology
University of North West

December 2001

Preface

This dissertation presents work conducted at the Materials Research Group of the iThemba Laboratory for Accelerator Based Sciences formerly known as National Accelerator Centre in Faure, South Africa from January to December 2001, under the supervision of Dr C. C. Theron and Co-supervision of Dr G. Dollinger.

Acknowledgements

I would like to take this opportunity to express my appreciation to the following people:

- Chris Theron, my supervisor, for his guidance and many helpful discussions.
- Guenther Dollinger, my co-supervisor, for his valuable inputs throughout this work and encouragement always.
- Karl Springhorn for helping me through out this work.
- Lawrence Ashworth for his technical expertise and interest shown.
- Solomon Marsh and Linda Ngobese for helping with their technical drawing expertise.
- Colin Doyle for always helping out when the PC was not coorparative.
- Jaynie Padayachee for taking the trouble of reading through all my work and helpful contributions.
- All the members of MRG for their moral support.
- Peter Mokoduwe, Pogisho Maine and Kenny Nkuna for everything, gens I know it was irritating and thanks.
- Johan Kritzinger for his valuable contribution to this work
- My family for always being there when I needed them.

Thank you.

Abstract

The characterization of materials is an important feature in the development of technologically important materials. The aim of this study was to contribute to the implementation of Elastic Recoil Detection (ERD), using a time of flight versus energy (TOF-E) detection system, as a tool to be used in the analysis of elastically recoiled ions from thin films. Energetic heavy ions from the Second Single Pole injector Cyclotron (SPC2) at iThemba Laboratory for Accelerator Based Sciences are used as the bombarding particles. The focus of this study was to construct the time of flight detector and to demonstrate that useful signals can be detected. The TOF-E detector is described and the time of flight for the alpha particles of energy 5.4 MeV was successfully measured to be 30 ns.

Table of Contents

List of Abbreviations

ERD	Elastic Recoil Detection
ΔE-E	Change in Energy versus Energy
iThemba LABS	iThemba Laboratory for Accelerator Based Sciences
L/D	Length to Diameter
MCP	Microchannel Plate
NECSA	Nuclear Energy Corporation of South Africa, Pretoria, South Africa
OAR	Open Area Ratio
RBS	Rutherford Backscattering Spectrometry
SIMS	Secondary Ion Mass Spectrometry
SPC2	Second Single Pole injector Cyclotron
SSC	Separated Sector Cyclotron
TOF-E	Time Of Flight versus Energy
UHV	Ultra High Vacuum

CHAPTER 1

1.1 Introduction

Characterization of materials is an important aspect in the development of technologically important materials. The quantitative and sensitive analysis of light elements in thin films has proven to be a major task since light elements play an important role modifying the surface properties of solids **[Gro 83, Hab 92, Guj 87, Hon 99, Hon 97B, Sto 89, Tir 96, Hon 97A, Mar 94, Grö 92,Zha 99, Kol 93]**. Thin film materials play a significant role in modern research and technology. It is therefore important to understand the structure and the elemental profiles of the thin films. Although many techniques exist such as Rutherford Backscattering Spectrometry (RBS), Particle Induced X-ray Emission (PIXE) etc, to investigate the structure of thin films, there is a lack of sensitive techniques for profiling light elements. One of the sensitive techniques is Secondary Ion Mass Spectrometry (SIMS). SIMS is in most cases a very sensitive technique but generally suffers from matrix effects, e.g. at surfaces and interfaces, which disturb quantification to a large extent. With SIMS a depth profile can be obtained, although preferential sputtering (dissimilar sputtering yields for different target atoms) is a problem **[Maa 98]**.

Characterization using accelerator-based ion beam analysis techniques is of critical importance in many laboratories. Two techniques are routinely used for materials characterization. Rutherford Backscattering Spectrometry (RBS) is a well-established technique that is mainly useful for analysis of heavy elements. It has several advantages, e.g. it is a non-destructive technique, has the ability to give reliable depth resolution and depth profiles of several elements simultaneously. However its inability to profile light elements in a heavy matrix is one of its limitations. ERD gives excellent elemental profiles for light elements retaining the advantages of RBS **[Boh 98, Maa 98]**. Unlike RBS where the scattered projectile ions are detected and analyzed, in ERD it is the recoiling target atoms that are detected and analyzed (see Fig 1.1). RBS is particularly sensitive to heavy ions, which gives ERD complimentarity over RBS in that depth profiling of light elements can be achieved with ERD.

The ERD technique was demonstrated in 1976 when J. LÉcuyer and coworkers **[LÉc 76]** described for the first time an analytical method based on detecting light elements recoiling at forward angles from a thin target after elastic collisions with an incident ion beam (25-40 MeV ^{35}Cl). They investigated lithium-containing thin layers (LiF or LiOH) separated by a copper layer (thickness of 30-150 nm) deposited on a carbon or copper backing **[LÉc 76, Tir 96]**. They were able to achieve a depth resolution of approximately 30nm, and the estimated ultimate sensitivity was as small as 10^{14} atoms/cm^2, thus introducing ERD as a sensitive analysis technique.

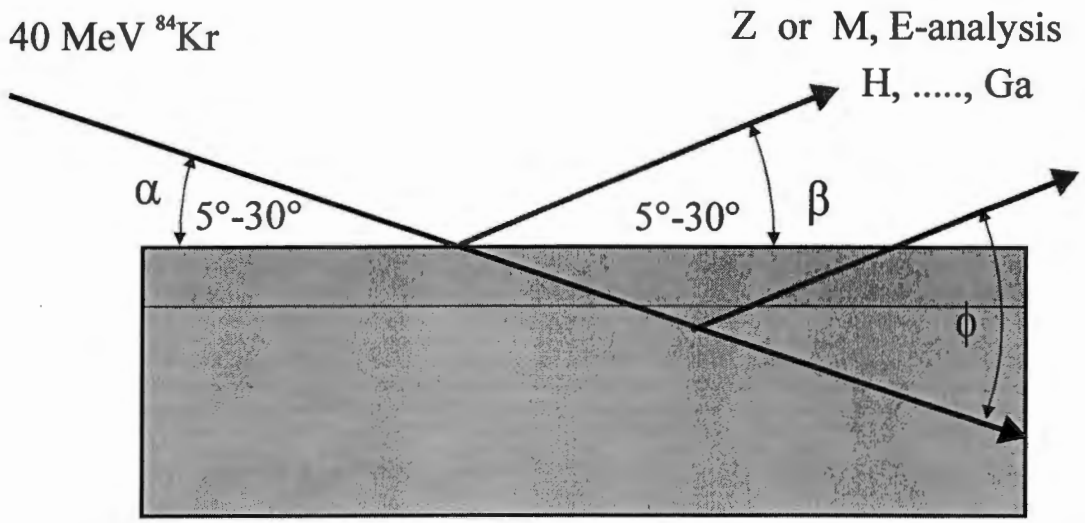

Fig 1.1 Schematic representation of an ERD setup using energetic heavy ions. Recoil ions scattered off by energetic heavy ions impinging at glancing angles to the sample surface are analyzed at forward directions for their mass or nuclear charge and energy.

1.2 Motivation of the Study.

The Materials Research Group at iThemba Laboratory for Accelerator Based Sciences (iThemba LABS) plan to implement ERD as a tool to be used in the analysis of elastically recoiled ions using energetic heavy ions from the Second Single Pole injector Cyclotron (SPC2).

This was motivated by the fact that the ions from the SPC2 would be ideal for ERD using a TOF-E detection system to be able to characterize thin films for profiling of light elements. Heavy ions from the SPC2 cyclotron with energies between 0.1 and 1 A MeV could be used and a TOF-E detector should analyze

recoil ions scattered off thin films. As part of the overall build up to introducing ERD using a TOF-E detection system, the focus of this study was (1) to construct the time of flight detector and (2) to demonstrate that useful timing signals can be detected.

1.3 Background of iThemba LABS and placement of ERD system.

The iThemba LABS is a multidisciplinary research laboratory administered by the National Research Foundation providing facilities for basic and applied research using particle beams, particle radio therapy for the treatment of cancer and supply of accelerator-produced radioactive isotopes for nuclear medicine and research. Activities are based around four sub-atomic particle accelerators. The large k=200 separated sector cyclotron accelerates protons to energies of 200 MeV, and heavier particles to much higher energies. Charged particles to be accelerated are fed to it via one of two smaller injector cyclotrons, one providing intense beams of light ions, and the other, beams of polarized light ions or heavy ions. The fourth accelerator at iThemba LABS is a 6MV Van de Graaff electrostatic accelerator.

There are mainly two suggested possible positions (see fig 1.2). One place (denominated as A) is just in front of the brick wall directly fitting into the transfer line to the SSC. It has the advantage that no additional beam line has to be installed. The disadvantage is that of probably not very good time resolution of the beam and that access to the ERD chamber is far away from a possible place for data acquisition and sample preparation. The more preferable place would be the place B. Its distance to the first rebuncher along the transfer beam line allows the usage of that rebuncher and therefore shorter pulse lengths. The other advantage is that the ERD setup would be in a separate room with ideal conditions for ERD

measurements. Even data acquisition and small target preparation and handling systems could be included and kept within small distances. The disadvantage of this position is that an additional beam line has to be installed including the bending magnet, a quadrupole doublet and an additional high vacuum pump.

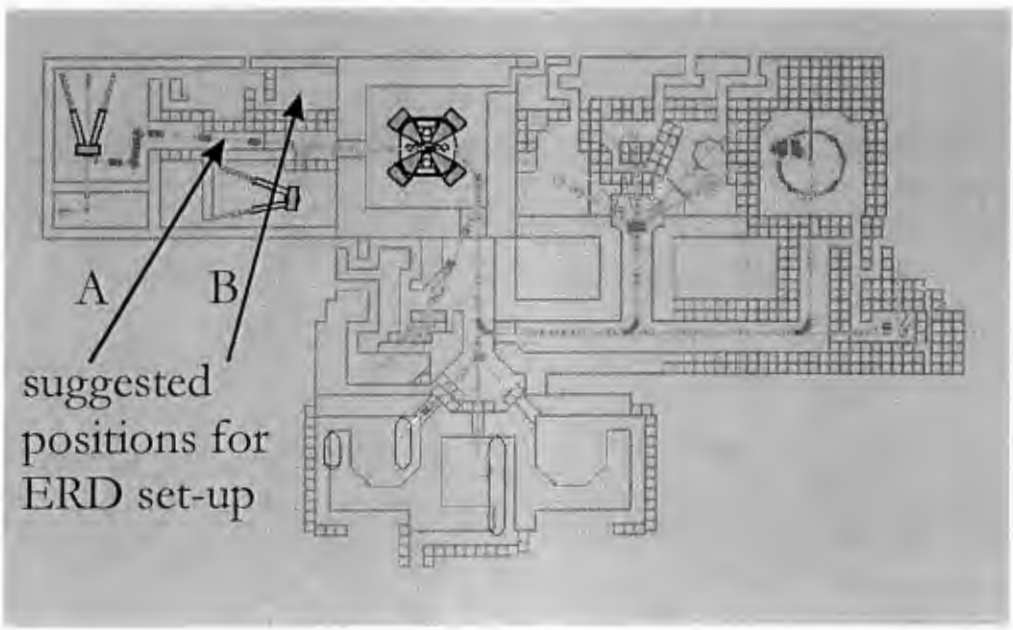

Fig 1.2 Floor plan of the cyclotron facility at iThemba LABS with the 2 positions indicated as A and B

1.4 Outline of the Dissertation

In **chapter 2**, a brief background of ERD is discussed with particular focus on ΔE-E and TOF-E detection systems. The design of a TOF-E detection system is also described.

In **chapter 3**, the design considerations of the TOF-E detector, which was constructed, are discussed. It mainly covers the test done on the detectors to check for voltage stability. The electronic and chamber arrangements are described and the test results are presented.

In **chapter 4** the first measurements made by the system are presented. A description of the start-up procedure for the timing detectors is included.

Results are summarized and future work is described in **chapter 5**

CHAPTER 2

2. Background/Theory

2.1 Elastic Recoil Detection

ERD using energetic heavy ions overcome many problems associated with light element detection in thin film analysis **[LÈc 76, Sto 89, Ass 96].** In a typical ERD experiment, recoil ions from the sample scattered off a thin film (see Fig 2.1) by an energetic heavy ion beam impinging the surface at glancing angles, are detected in the forward direction and analyzed for their nuclear charge or mass and energy. The well-known cross sections and stopping powers for the incident and recoil ions gives the opportunity to calculate depth profiles of the elements in a thin film layer from the elemental energy spectra. The recoil ions lose energy during the travel in the surface that is proportional to their stopping powers, which are energy dependent. The energy of the detected ion E_2 is related to the mass M_1 and energy E_0 of the incident ion through the kinematic factor

$$K = \frac{E_2}{E_0} = \frac{4M_1M_2}{(M_1 + M_2)^2}\cos^2\theta \qquad \text{---- (1).}$$

The Coulomb cross section for ERD is given by

$$\sigma = (\frac{Z_1 Z_2 e^2}{4E_0})^2 \frac{4}{\cos^3\theta}[\frac{M_1 + M_2}{M_2}]^2 \quad \text{----(2).}$$

where M_2 is the mass of the recoil ion, θ is the recoil angle and e is the electronic charge **[Guj 87]**. Knowledge of the kinematic factor, the scattering cross section and the stopping power allows full characterization of the spectrum.

ERD is used in many laboratories and it has been proven to successfully and repeatedly deliver quantitative depth profiles of light elements in thin films **[Ass 96, Guj 87, Tim 98, Boh 98, Ber 98]**.

2.2 Methods of Detecting the Recoil Atoms

There are two main detection methods used to profile all elements simultaneously in standard ERD experiments.

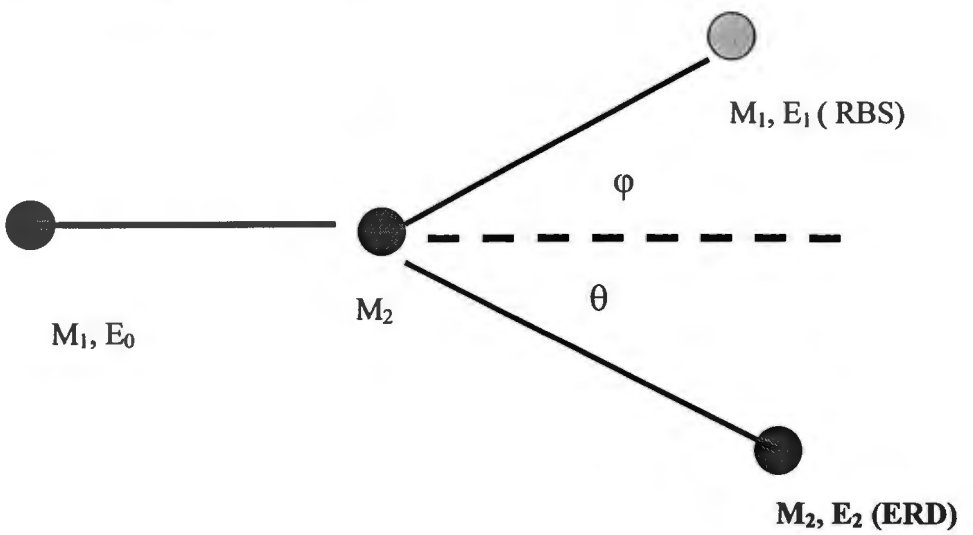

Fig 2.1. Scattering process for ERD and RBS, where φ is the scattering angle measured with respect to projectile direction and θ is the recoil angle measured with respect to the projectile direction.

2.2.1. ΔE-E detector

The first technique uses the recoil energy loss in combination with a residual energy measurement to do mass separation **[Ass 96, Tim 98, Ber 98]**. The ΔE (energy loss) signal is measured by a thin detector (e.g. an ionization chamber Fig 2.2 **[Dol 98]**) and the residual energy is measured in a subsequent thick detector (e.g. a silicon detector) in coincidence. Since lower- energetic recoils are readily stopped in the ΔE detector **[Maa 98]**, these techniques require high ion beam energy to be able to measure ΔE and the residual energy to achieve elemental separation. It is therefore often used at heavy ion accelerators that deliver high-energy heavy ion beams, e.g. large cyclotrons or tandem accelerators.

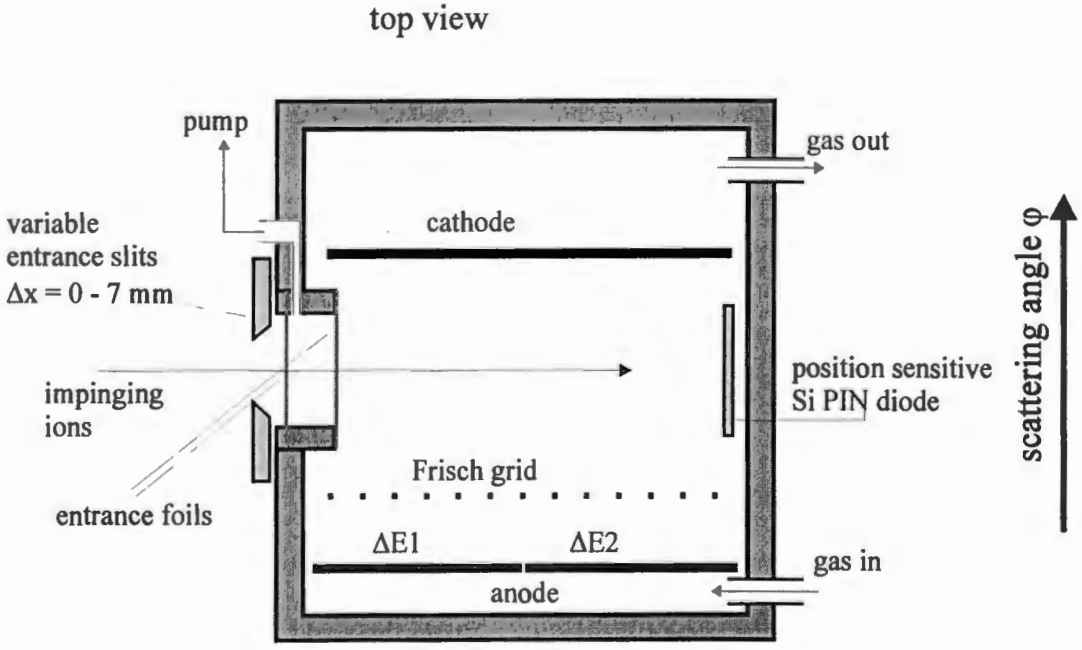

Fig 2.2 A typical arrangement of an ΔE-E experimental setup. The impinging ions loose energy as they traverse through the ionization chamber and the residual energy is measured at the Si PIN diode.

Fig 2.3 shows an ERD spectrum of 24x 10^{17} at/cm^2 of $(Al_{0.2}\ Ga_{0.8})N$ layer on an Al_2O_3 substrate. Fig 2.4 is a depth transformation of the elemental separation from Fig 2.3.

The elemental separation using a ΔE-E detector system is good at high energies but at lower energies separation is not possible. With such an ionization chamber (Fig 2.2), ΔE-E is unable to separate masses at energies < 1MeV/nucl. One solution would be to use more energetic ions so that the recoils with energies < 1 MeV/nucl only come from the substrate. However some samples (notably oxides) might get destroyed before the measurement is completed and enough information is obtained from the sample, since irradiation damage is more severe with energetic heavy ions, alternatives that reduce irradiation damage must be investigated.

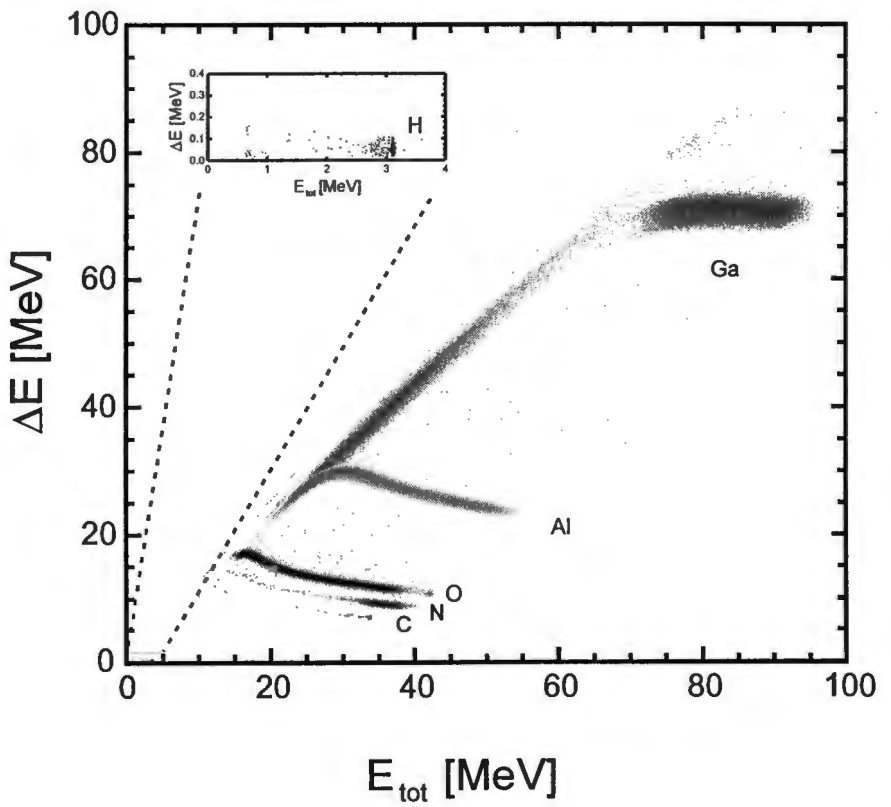

Fig 2.3 Spectra showing the elemental separation using the ΔE-E detector. **[Dol 98]**

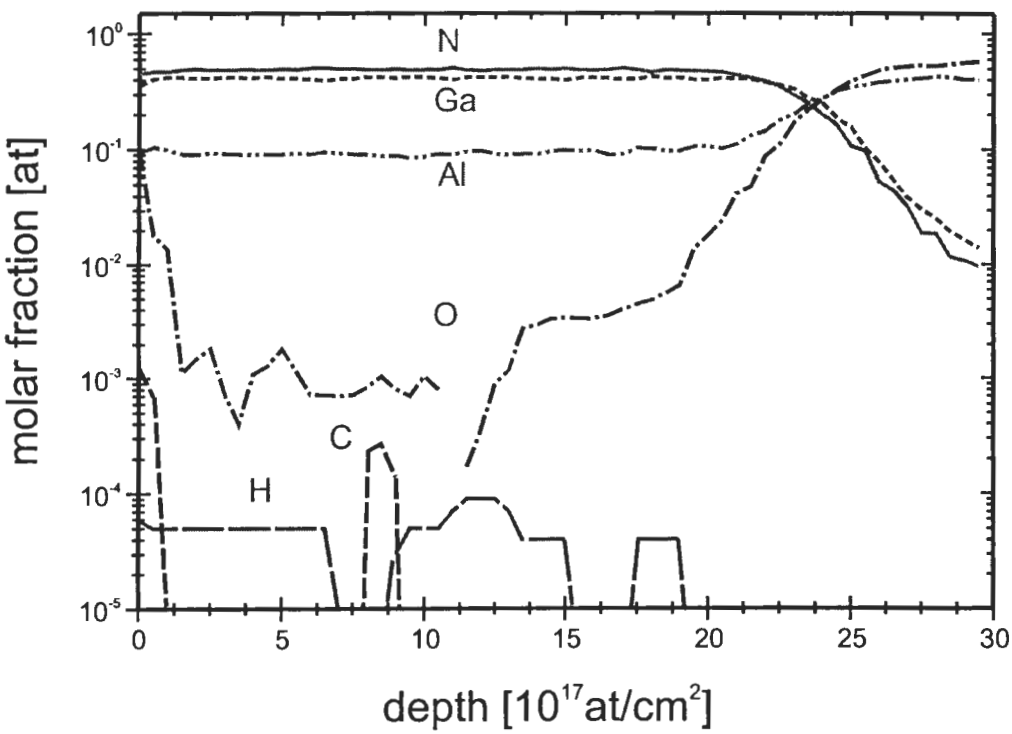

Fig 2.4 Depth profiles transformation from the spectra in Fig 2. 3. **[Dol 98]**

2.2.2 TOF-E Detector.

Irradiation damage is a principle problem in ERD analysis. Irradiation damage increases with energy since the ratio of the damage and detection cross-sections increase even if only nuclear stopping is considered **[Dol 92]**. By reducing ion energies the damage for materials sensitive to electronic stopping effects is significantly reduced **[Dol 96]**.

The use of heavy ions with lower energies (0.1-1MeV/nucl) provides a solution to the problem of irradiation damage and keeps the advantages of ERD. The ions from the SPC2 at iThemba LABS are ideal for this purpose, however the ΔE-E method is no longer viable, because at energies <1MeV/nucl. (Fig 2.3) heavier recoils will not be resolvable. The alternative method is time of flight TOF-E for a general purpose ERD, which is ideal at these energies. This can be observed in Fig 2.6 that even at energies <1MeV/nucl elemental separation can still be attained.

A TOF-E measurement are made when the recoil passes through two thin carbon foils and gets stopped in the surface barrier detector. When the recoiled atom passes through the carbon foils, secondary electrons are emitted and accelerated by an electric field to microchannel plates (MCPs). Electrons are multiplied in the channels of the MCPs and a fast time signal is generated. The difference in time between the signals from the two foils is the time of flight (TOF) of the recoil. After passing through both foils the energy of the recoil, E, is measured in a solid-state particle detector.

The mass of the recoiled ions is related to the TOF and E of the particle by the following relationship

$$M = 2E\frac{(TOF)^2}{l^2} \qquad \text{- - - - (3)}$$

l is the flight path that the recoils cover between the two foils.

2.3 TOF-E Detection.

The construction of the time of flight detector formed an integral part of this work, since this detector is to be used for ERD at the Injector cyclotron SPC2 at iThemba LABS for thin film analysis. Fig 2.5 shows the arrangement of the time of flight detectors (TOF-E) for ERD measurements. The timing signals from the two-stage channel plates together with the energy signals from the silicon detector will allow elemental separation.

Two different TOF measurements will be used in the final set-up. One is a precise TOF measurement for the heavier recoil ions ($Z \geq 3$) using signals from the carbon foils and the other is the TOF measurement using the timing signal from the cyclotron for the hydrogen isotopes.

For ($Z \geq 3$), the TOF will be measured between two thin carbon foils, separated by the desired path length (l=0.46m), which emit secondary electrons on ion bombardment. These electrons are accelerated by an electric field and multiplied by the channel plate detectors (Fig 2.5). The sensitivity for detection of elements with $Z \geq 3$ is about unity and can be easily calibrated. The expected timing resolution is better than 200 ps at a TOF of about 50 ns. It gives the necessary resolving power to resolve single atomic masses even for heavier elements. In addition at low ion velocities (energies), it allows better energy resolution and therefore depth resolution compared to the energy resolution obtained from the silicon detector.

The electron coefficient (number of secondary electrons per ion) is low for hydrogen recoils (only some few 10%) and may vary with time of measurement due to changes of the carbon foil surfaces. Therefore an alternative measure is to be employed for hydrogen recoils in order to get large and stable sensitivity also for the hydrogen isotopes.

The SPC2 Injector cyclotron produces a pulsed beam with the pulses coming at a constant time interval. For hydrogen recoils TOF will be measured by correlating the timing signal of the silicon detector with the timing signal of the beam pulses of the Injector cyclotron. The timing resolution is expected to be only in the range of 5 ns, but it will be sufficient to resolve hydrogen isotopes and the detection efficiency will be 100%.

Both carbon foils have been rotated relative to the normal position: by the scattering angle φ. The rotation of the first foil compensates for changes of times of flight and changes in the kinematics due to an extended beam spot, while the rotation of the second foil makes a first order correction for ions scattered off at the surface towards different angles. **[Dol 01]**

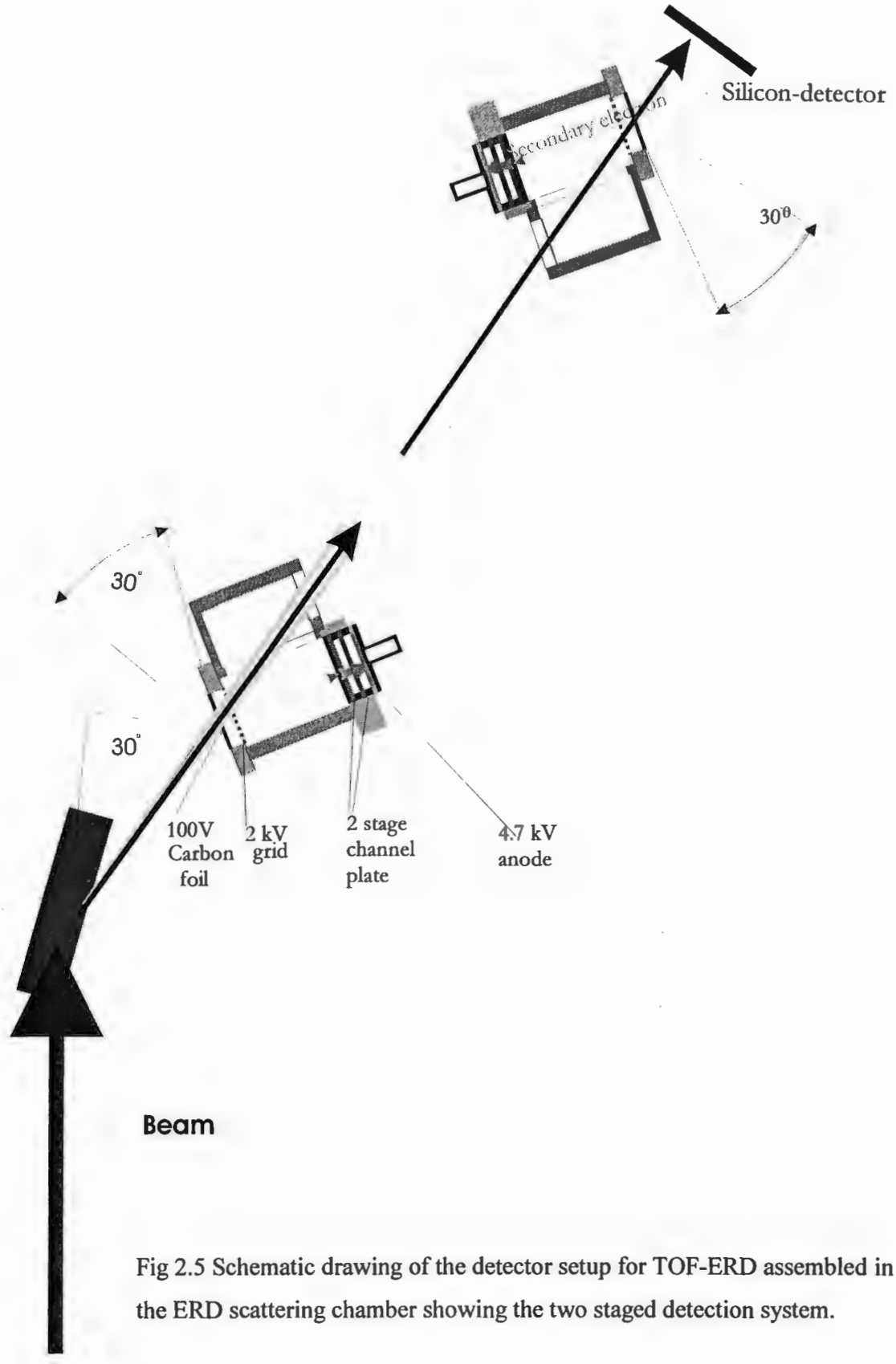

Fig 2.5 Schematic drawing of the detector setup for TOF-ERD assembled in the ERD scattering chamber showing the two staged detection system.

Fig 2.6 shows elemental separation obtained with a TOF-E detector, which shows that even at lower ion energies there is a good elemental separation **[Boh 98]**. This is a t_0 -TOF versus energy of the recoiled particles, where t_0 is the time delays of the whole set-up **[Boh 98]**. This elemental separation can also be transformed into depth profiles as with the ΔE-E measurement.

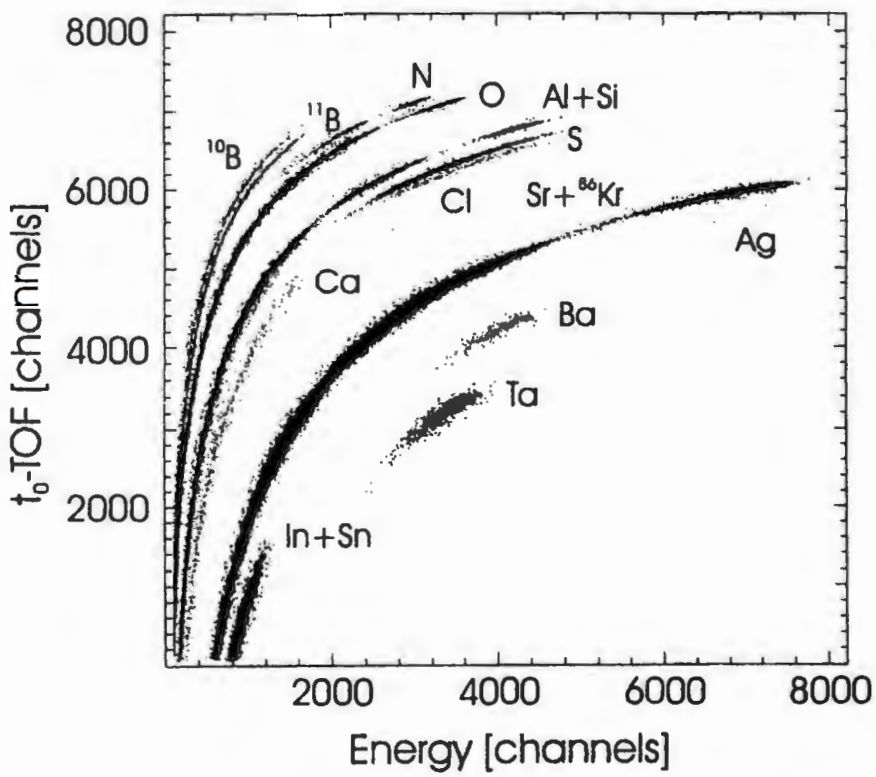

Fig 2.6. Energy vs. (t_0-TOF) spectrum measured at 40^0 for a multiple layer sample (ITO, ALON< SrS: Ag, ALON, BaTaO on borosilicate glass) with a beam of 120 MeV ^{86}Kr. **[Boh 98]**.

CHAPTER 3

3. Design considerations of TOF-E Detector

3.1 Introduction

The ERD experimental facility will be setup at the transfer line between SPC2 and the Separated Sector Cyclotron (SSC) at iThemba LABS. It will be used as a general-purpose setup to analyze depth profiles of light elements in thin films. Heavy ion beams of the SPC2 cyclotron with energies between 0.1 and 1 A MeV will be used and recoil ions scattered off thin films will be analyzed by a detector and a silicon detector in coincidence at a recoil angle of about 30^0as described in section 2.3 and shown in Fig 2.5 of the previous chapter.

In order to have good performance for ERD measurements a good time resolution of the system is necessary. The detection system consists of two timing detectors, one situated close to the target and one just in front of the silicon detector with flight paths adjustable between 0.46m and 1m length. The two timing detectors are specially designed for fast timing of swift ions and are identically constructed at the moment. The working principle of the detectors will be discussed in the following chapter.

When a recoil particle passes through a timing detector it hits a thin carbon foil, which emits secondary electrons. The thickness of the foil should be as thin as possible in order to reduce energy straggling and small angle scattering. Although secondary electron emission reduces for thickness below an equilibrium thickness of several $10\mu g/cm^2$, the thinnest obtainable foils ($0.6\mu g/cm^2$) should give a sufficient electron yield **[Hab 92, Lie 97]**. However, for the first tests mechanically more stable $11\mu g/cm^2$ carbon foils were used. The carbon foils were produced by P. Maier Komor from Technical University of Munich and mounted at iThemba LABS on stainless steel frames with an aperture of 9.5 * 12 mm^2.

The foils are prepared in three different ways and the mounting process for each is described. Foils on Betaine are mounted by placing them at an angle (about 30^0) and letting them to float in distilled water, which is slowly run in the water bath and then they are mounted on suitable frame. Foils on Lensodel: Heat them in normal environment at 200^0C for two hours and then proceed as explained above. Foils on Lensodel + copper: Heat them in normal environment at 200^0C for two hours and then float them in water like for the foils on Betaine, after floating the copper-carbon layer in distilled water, the foil is mounted on a 1mm thick Teflon sheet to transfer it into a vessel filled with acid for dissolving the copper. Two different acids are used, both with good success. In 50 ml water 10 g of trichloro acetic acid were dissolved and 50 ml ammonia were added. The other acid consists of 4 parts of water mixed with one part of highly concentrated (65%) nitric acid. After dissolving the copper, the carbon foil is again transported via the Teflon sheet to a fresh distilled water bath, from where it is mounted on a suitable frame.

The emitted secondary electrons are accelerated by an electric field into the MCPs, which act as electron multipliers. A two-stage system is used giving a total gain of about 10^7 or 10^8 electrons depending on the type of MCP used.

To avoid damage to the MCPs the detectors had to be first tested for voltage breakdown without the MCPs. When stability was achieved, the MCPs were introduced and the detectors were tested again.

This chapter gives a detailed description of the considerations made when designing the TOF-E detector. It introduces various options for assembling the detector with particular focus on the choices made in this work. The voltage breakdown tests of the detector and the results are discussed. The ERD chamber is described at the end where the TOF detector is installed and tested.

3.2 Detector Assembly.

There are a number of considerations that should be taken into account when designing, assembling and testing the detector: the choice of the materials to be used and the way the detector was assembled.

Fig 3.1 shows the standard/manufacturer's options for mounting the microchannel plates. There is more than one option available for consideration when assembling the detector depending on what is required (Fig 3.1). There is a single MCP (one plate mounted) giving a gain of up to 10^3or 10^4 electrons depending on the type of MCPs used on the output side with a bias voltage of 1000V. Another is a chevron (two MCPs mounted) giving a gain of up to 10^6 electrons on the output side of the channel plate with a bias voltage of 2000V. The last one is a Z- stack (three MCPs mounted) giving a gain of up to 10^7 electrons with a bias voltage of 3000V.

Based on the suggestion by Kasülke **[Kas 94]** a different approach was used in this work of using two single MCP with a 300V potential applied between them (see Fig 3.2). This acceleration voltage between the two MCPs has two positive effects. It increases the gain of a two-stage setup since all electrons from the exit of the first channel plate are collected at the second and amplification from these 300 eV electrons is obtained. Therefore, a similar amplification as a 3-stage channelplate arrangement is obtained. The second effect is a reduction of pulse width due to a fast and definite transition time from one MCP to the other and due to an overall reduction of traveling distance for the electrons.

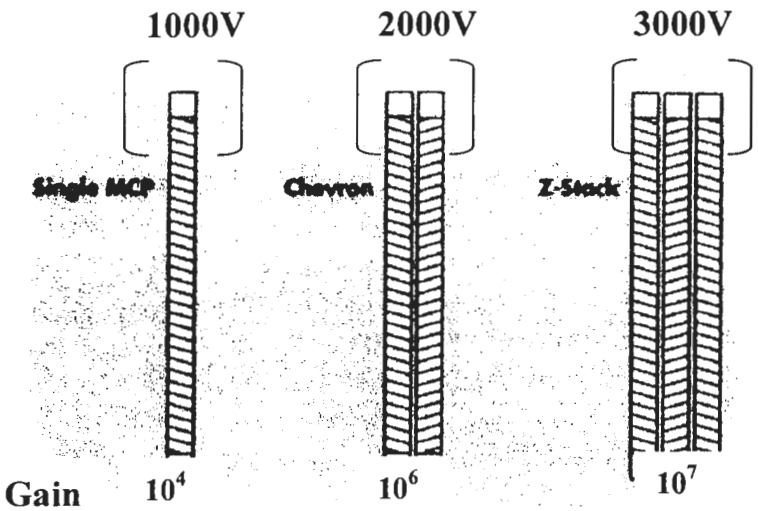

Fig 3.1. Manufacturer's standard configuration of the already mounted MCPs, which can be used in time dependent methods. **[Bur]**

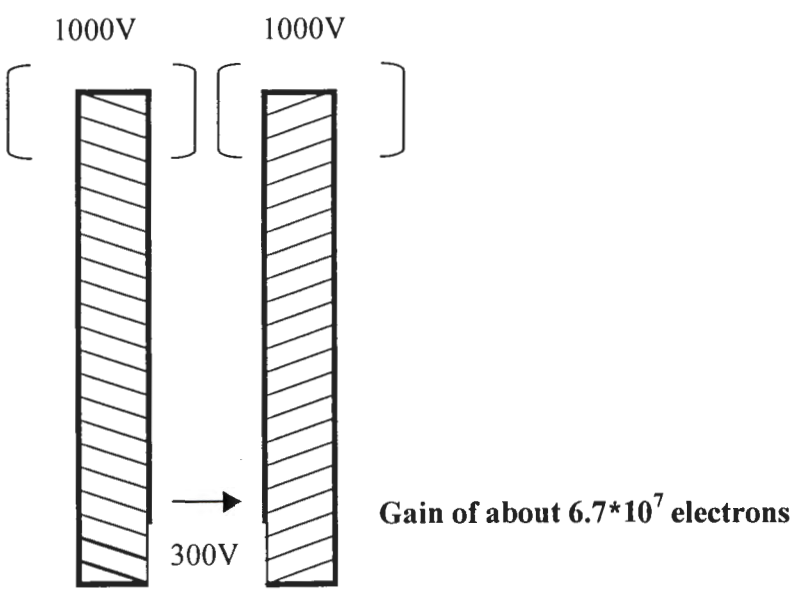

Fig 3.2. The proposed assembly of two single MCPs with a bias voltage of 300V between them.

	Burle	*Phillips*
Length to Diameter	60:1	40:1
Channel diameter	5μm	10μm
Center to center	6μm	12μm
Bias angle	5^0	6^0

Table 3.1 Specifications of the MCPs from *Burle* and *Phillips*

The specifications of the MCPs used in this work are shown in Table 3.1. To optimize the lifetime of the detector it must be operated at the minimum voltage necessary to obtain a usable signal.

The manufacturing process of the MCP begins with a specially formulated lead glass tube and solid core assembly that is drawn and fused to form an array. The fused array is sliced into wafers. The wafers are chemically processed to remove the solid core, leaving a uniform porous structure of millions of tiny holes or microchannels. Through further processing of the microchannel plate walls, an alkali, silica-rich secondary electron emissive layer is formed on an electrically semiconductive layer. Lastly a thin metal electrode is vacuum deposited on both the input and output surface to electrically connect all channels in parallel as can be seen in Fig 3.3 **[Bur]**.

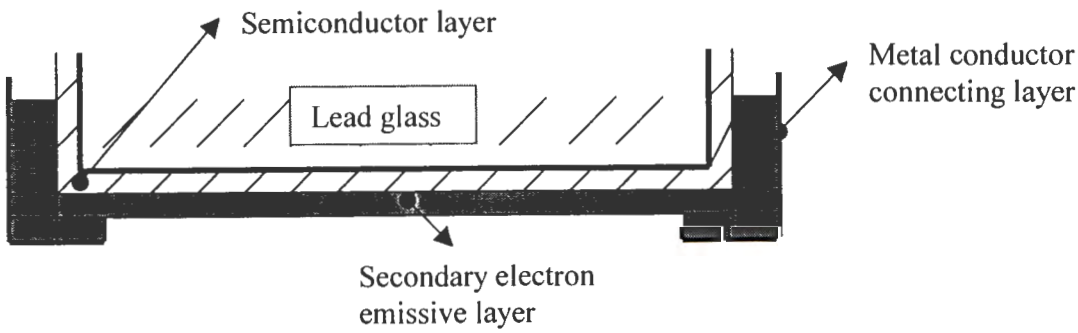

Fig 3.3. Showing the parts of the microchannel and how the microchannel is manufactured.

3.2.1 Multiplication Process

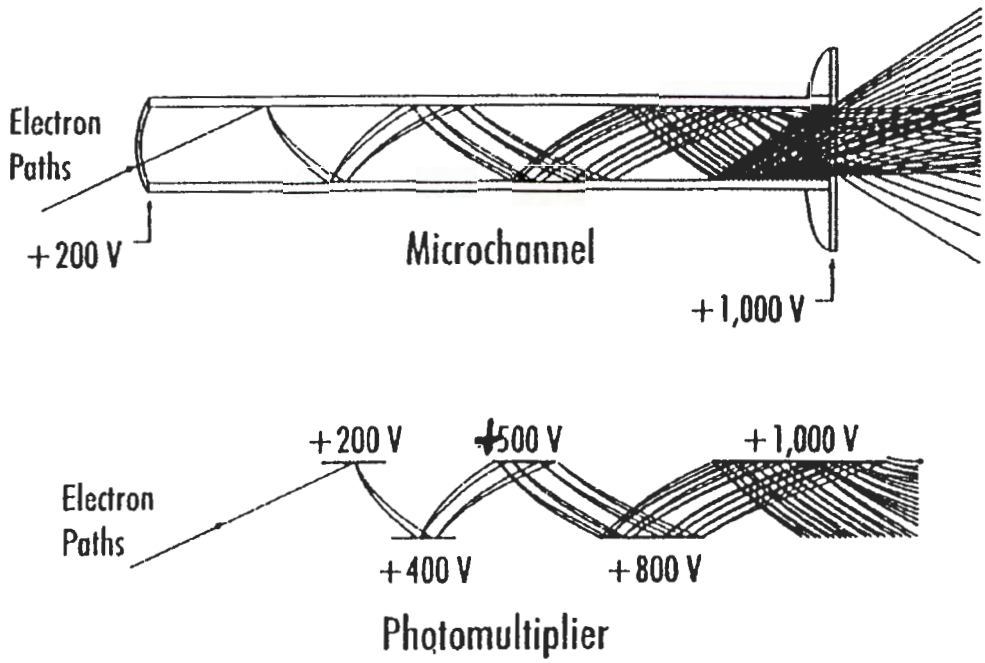

Fig 3.4 Showing how a michrochannel works analogously to a photomultiplier tube **[Rop].**

Microchannel plates are used in applications that are time dependent. Each microchannel functions as a channel electron multiplier, independent of the adjacent channels. For optimum operation a bias of up 1000V is applied across the MCP. The bias current flowing through the semi-conductive layer see Fig 3.3. supplies the electrons necessary to continue the avalanching multiplication process. The multiplication process is shown schematically in Fig 3.4 for a single channel. This process can be described as follows:

When incident radiation strikes the channel wall, on the input side of the channel, secondary electrons are generated and are accelerated down the tube. When they strike the channel wall again, further secondary electrons are generated. A gain of up to 10^4 electrons can be achieved on the output side of the channel. The detection efficiency is high when the pore size is small. The higher the open area ratio (OAR), the more efficient the detector is. However this also means that

MCPs with a high OAR are also extremely fragile. With 300V applied between the two MCPs the second MCP will see 300 eV electrons. As can be seen from Fig 3.5 these electrons are almost optimal in terms of detection efficiency. Increasing the bias voltage beyond 300V could increase the detection efficiency, but large changes should not be expected.

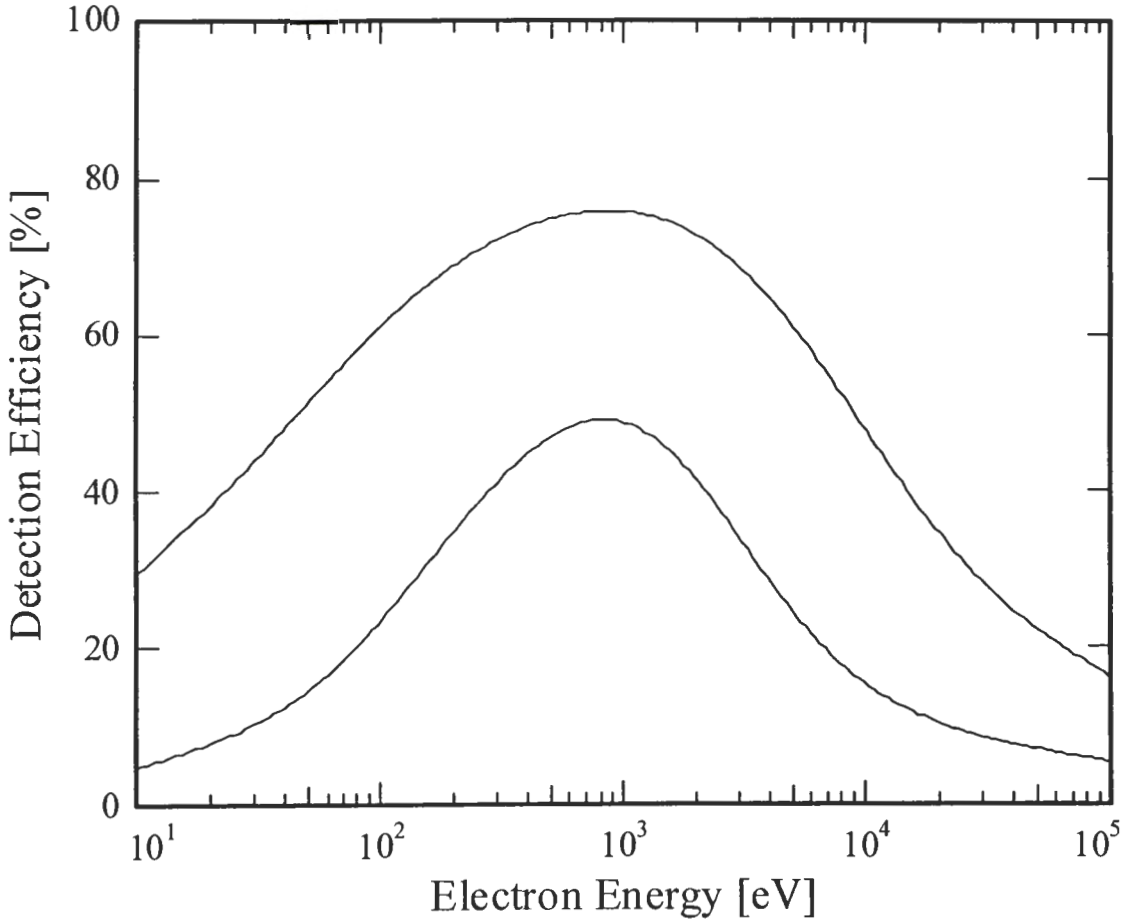

Fig 3.5 Showing the detection efficiency curve for electrons, which shows that electrons with energy of 300 eV give an efficiency of about 42%. **[Bur]**

3.2.2 Applied Voltages

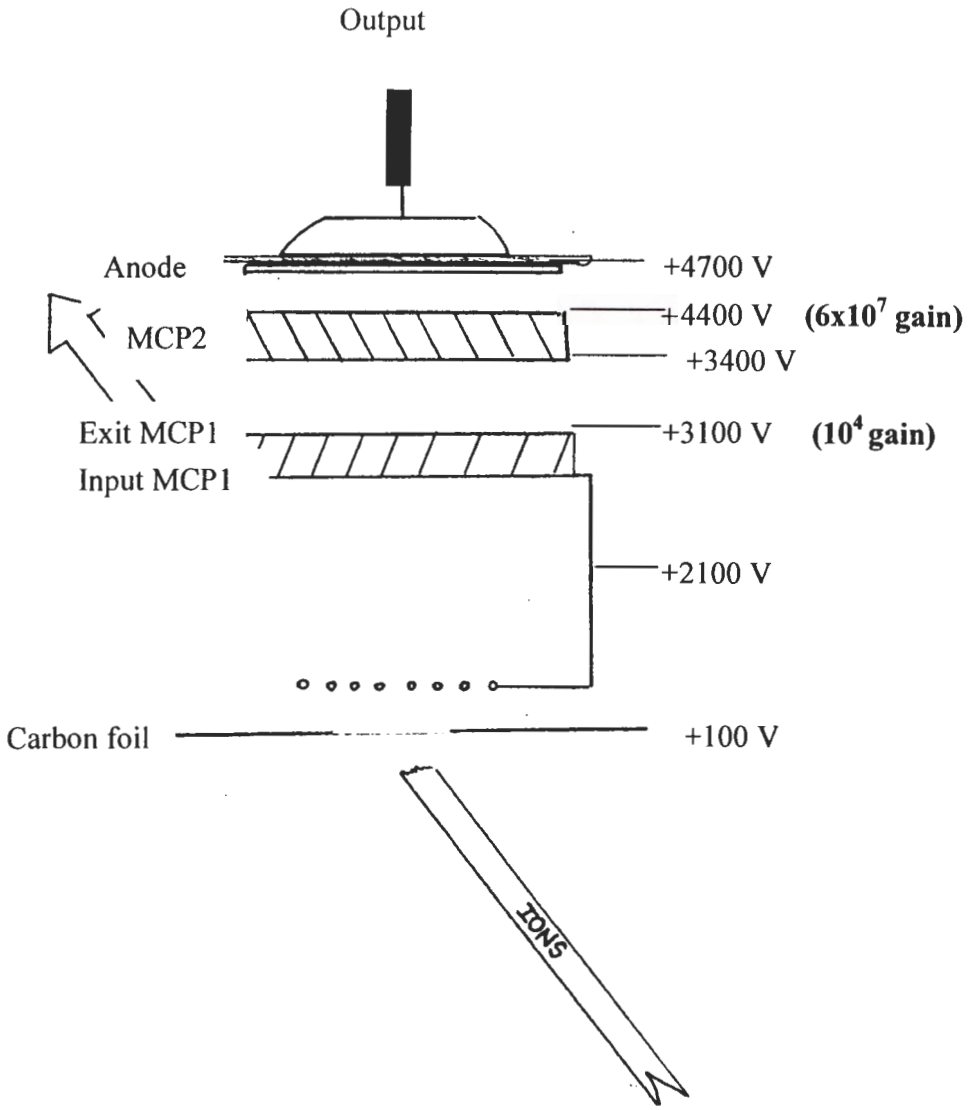

Fig 3.6. showing the assembly of the microchannel plate detector.

For optimum operation of the detector the applied voltages would be as shown in Fig 3.6. The resistor chain can however, be changed to give the voltages at which a usable signal can be generated from the detectors. The nominal voltages applied to the different parts of the detector are plotted in Fig 3.6. The voltages are generated from a 5 kV power supply using a resistive chain for voltage division.

The carbon foil is at 100V. The foil sits at 100V so as to avoid stray ions from getting into the detector. The grid and the entrance of the first microchannel plate are at 2100V. The exit of the first microchannel plate is at 3100V. The entrance of the second mirochannel plate is at 3400V and the exit is at 4400V. The anode is at 4700V.

3.3.Chamber

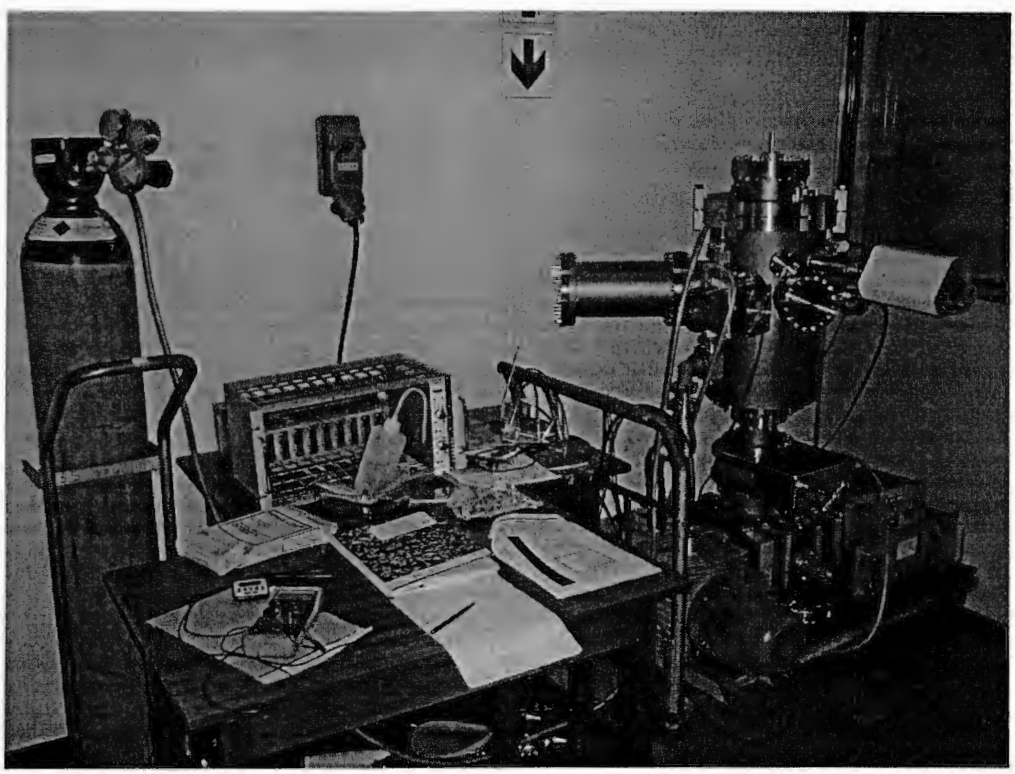

Fig 3.7. A photograph of the ERD scattering chamber.

The main requirements for the target chamber are a good vacuum in the UHV region ($<10^{-6}$ Pa), a 3(4) stage goniometer for sample manipulation, a load lock to change samples without breaking the vacuum and several flanges for installing the detector at 30^{0} intervals (a second port at 15^{0} should also be adapted) and to mount several electrical feedthroughs and view ports. The view ports are necessary especially to adjust position and angle of the sample. In this work an

UHV chamber from NECSA was used as an ERD chamber. It was modified to include certain flanges and valves to mount the TOF detector arrangement. It has a UHV pump (ion pump), a roughing pump and a turbo pump. It is able to give a vacuum of better than $9x10^{-7}$ mbar, which is suitable for ERD detector operation.

3.4. Electronics.

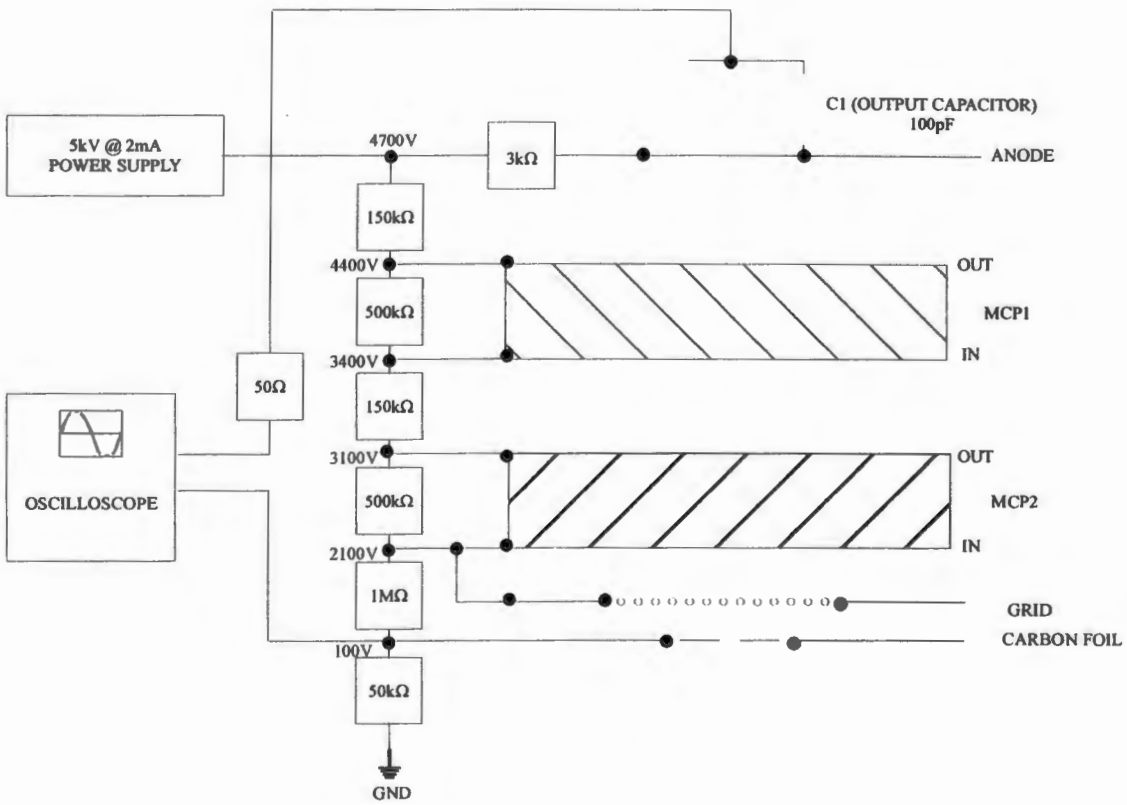

Fig 3.8 Schematic layout of the electronics used to test for breakdown in the detectors.

Fig 3.8 above shows a schematic representation of the arrangement for testing for voltage breakdown in the assembly using a power supply with 4700V applied voltage. The power supply was connected over a resistance chain (potential divider) that supplies the different potentials to the detector assembly. The power supply supplies a maximum current of 2mA. The observations were made using a

two-channel oscilloscope, one channel connecting the output capacitor via a 50Ω terminator, which was DC coupled, and the other connected to the carbon foil that was AC coupled.

3.5 Voltage Stability of the detectors without the MCPs mounted

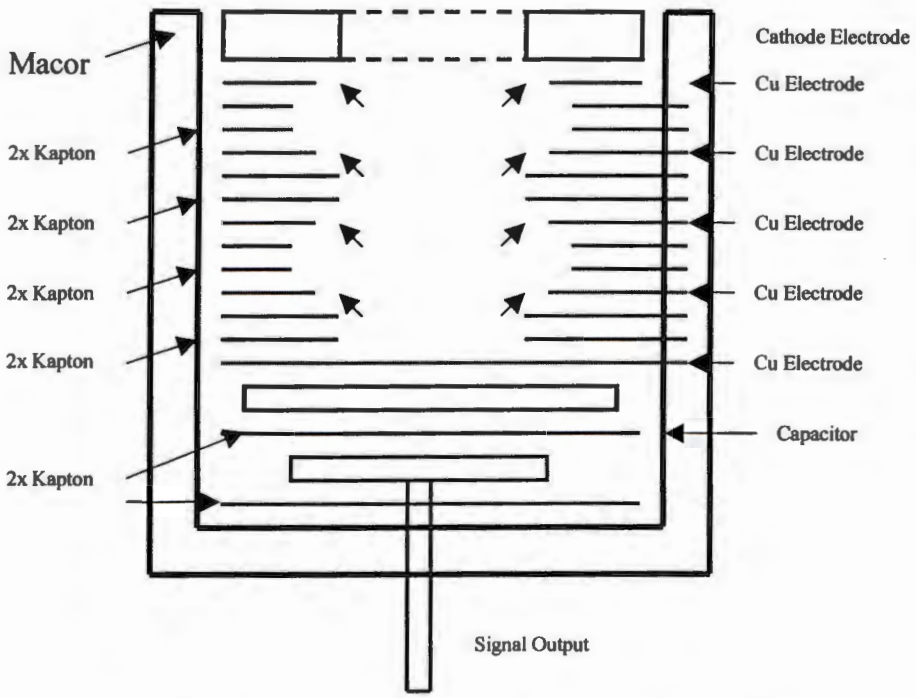

Fig 3.9. Showing the assembly without the microchannel plates

Fig 3.9. Shows the setup of the detector initially assembled without the MCPs when the voltage stability tests were done. Numerous discharges (see Fig 3.10) were observed. Removal of the MCP resulted in insufficient insulation of the Cu electrodes that are on the entrance and exit of the MCPs as can be seen in the Fig 3.9 and indicated by arrows. The kapton foils had a larger diameter and thus could not provide sufficient insulation on the Cu electrodes. This was improved by

replacing the kapton foils between the Cu electrodes (as indicated by arrows in Fig 3.9) with kapton foils with a small diameter to provide better insulation.

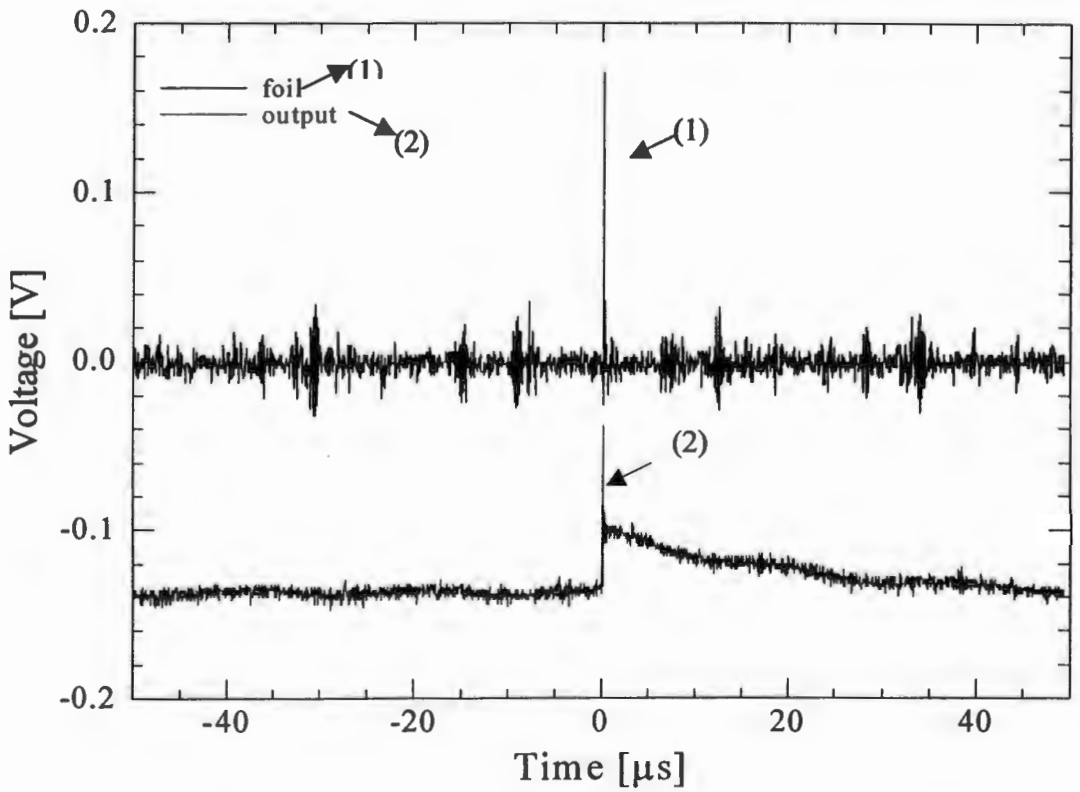

Fig 3.10. The results of the initial test for voltage breakdown. There numerous discharges observed. The output trace (2) has a long discharge time because the capacitor was not terminated with a 50Ω resistor.

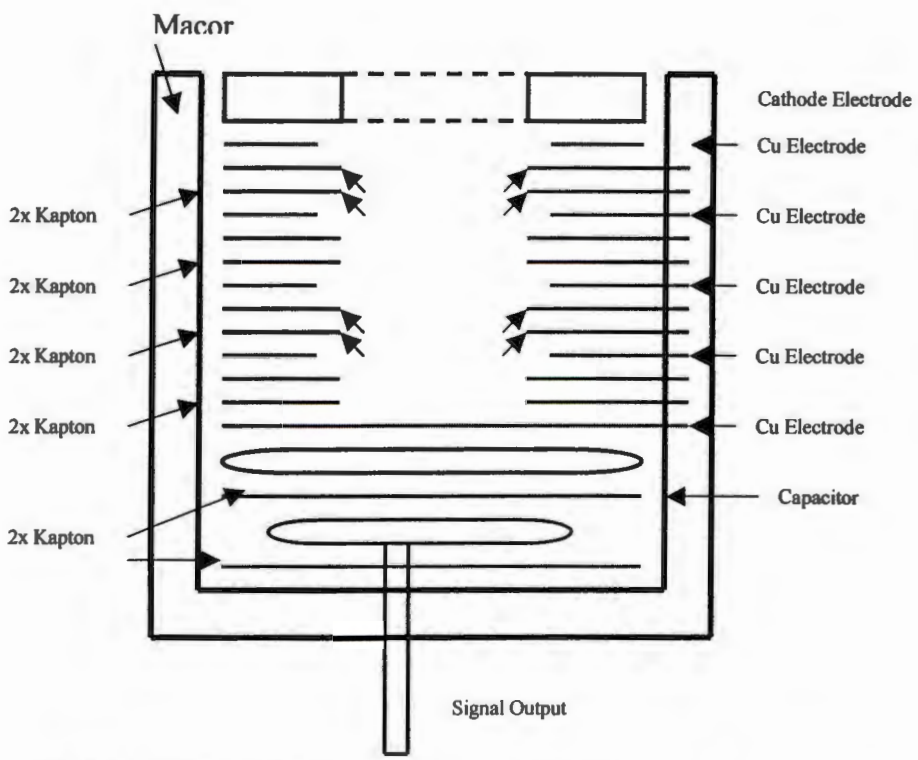

Fig 3.11. Showing the improved assembly for testing the voltage stability.

The modified assembly for testing the voltage stability with the kapton foils replaced is shown in Fig 3.11. Besides reducing the diameter of the kapton foils to provide sufficient insulation to the Cu electrode the following changes to the system were made: the edges of the stainless steel were rounded off to minimize the electric field strength on them. The resistors in the resistor box (potential divider) were too close to one another inducing discharges and were rearranged to increase the space between them. The shield caps were placed over the high voltage point of the feedthroughs to stop possible electron emission from them.

The shield caps were too short and had to be lengthened to stop discharges induced between the chamber and the feedthroughs.

Results of the changes can be seen in Fig 3.12 and this can be seen from the difference in the pulse height of the discharges. The output was measured with a 50Ω terminating resistor. 'Foil' means the measurements were made at the carbon foil, which was in this case the monitoring point sitting at 100V. The sharp pulse means that the discharges are at or near the carbon foil. This is because the capacitance of the system increases with increasing distance from the monitoring point and results in long response times. The long rise time pulse at the carbon foil test point as can be seen in Fig 3.12. (2) means that the discharges are at or near the high voltage region (at the 4700V anode).

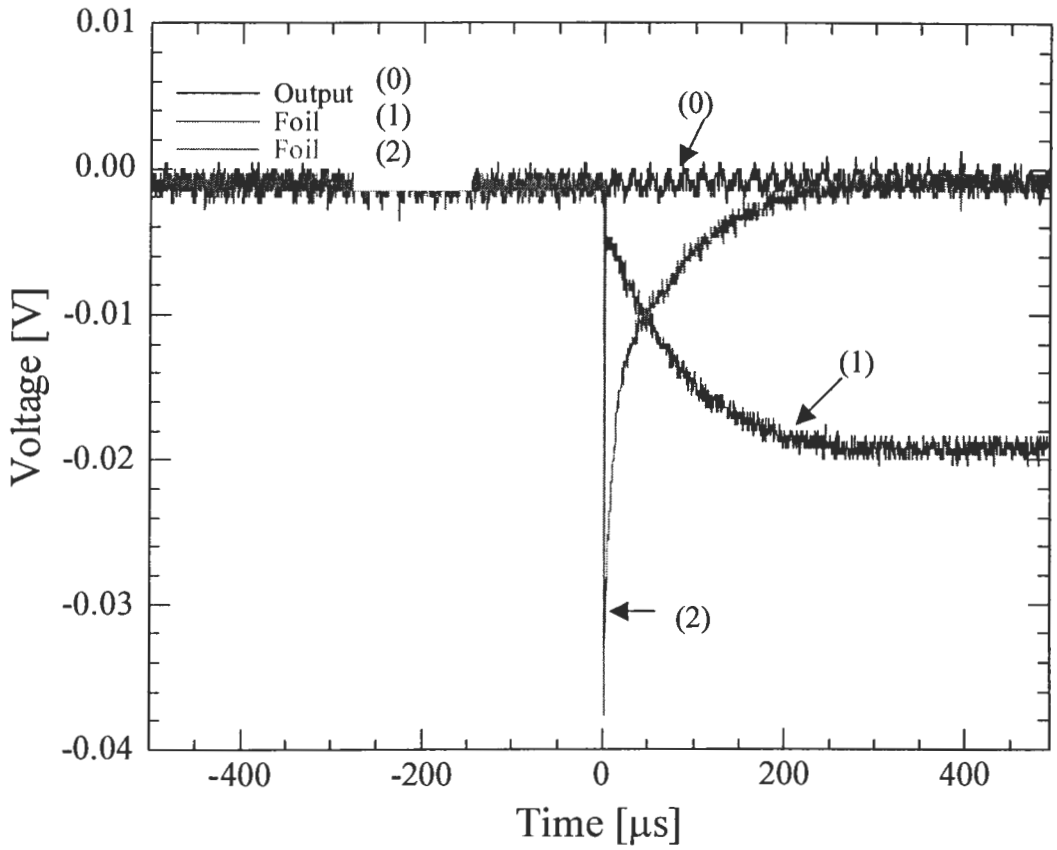

Fig 3.12. The tests result of the modified detector showing the pulses occurring at different places in the detector and observed at the carbon foil.

The tests before the system was improved showed discharges of about 180 mV at a high repetition rate. When the tests were done after improvements were made, the discharge level dropped to 40 mV at a frequency of about 5.5x 10^{-3} Hz, which was on average equivalent to one count per 180 seconds. This was found to be an acceptable level at which it is safe to mount the microchannel plates without causing damage to them.

3.6 Summary

The detectors were assembled without the MCPs to avoid chances of damaging them and the tests were done on the detectors. The system was tested after construction. Systematic tests were made after each modification to the design of the detector.

The improvements made to the system were to change the diameter of the kapton foils to achieve good insulation of the Copper electrodes. The edges of the stainless steel plates were rounded off to minimize the electric field effect. The distance between the resistors in the resistor chain box was increased. The feedthrough shield caps were modified to move them away from the feedthrough caps. With these improvements, system stability was achieved and further tests could be done on the system with the MCPs stacked in. The chamber was able to give a vacuum of better than $9x10^{-7}$mbar.

CHAPTER 4

4 First measurements

4.1 Introduction

The TOF-E detectors could only be assembled after voltage stability was reached when they were tested without the microchannel plates. The aim of this chapter is to demonstrate that TOF-E detectors can give pulses related to the time of flight of the particles traversing the flight distance *l*. The detectors were assembled with the MCPs mounted. The tests were done using an alpha source. The detectors were baked following the procedure described in section 4.4. The results are shown and discussed in section 4.5.

4.2 Implementation

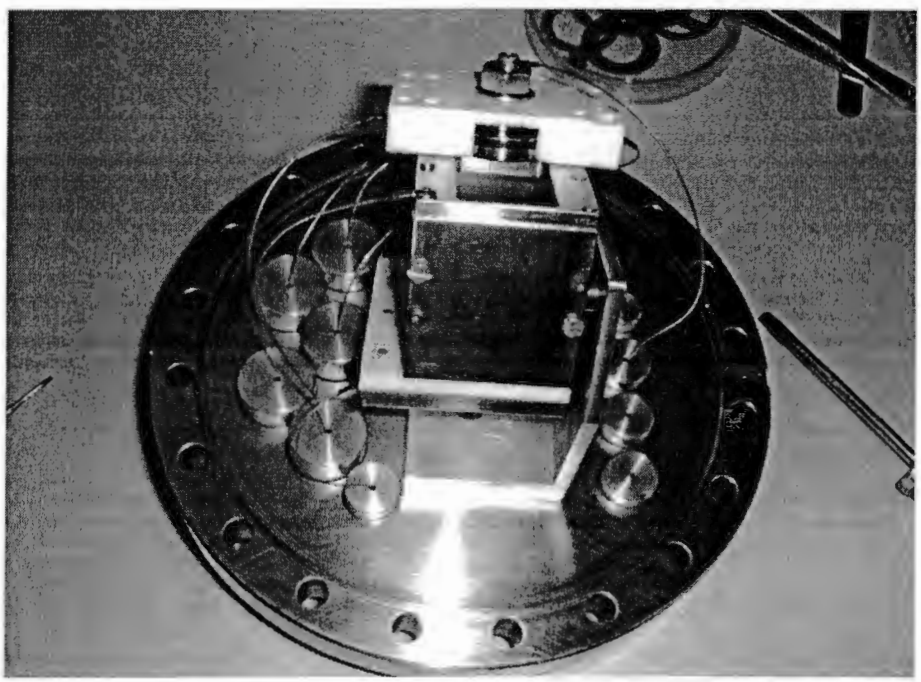

Fig 4.1 A photograph of the second timing detector mounted on the flange, to be used for TOF-E measurements.

The photograph in Fig 4.1 shows a picture of the assembled timing detector mounted on a flange. Wires to the left supply the high voltage to the detector from the resistor chain through shield caps. The wire to the right is connected to the output of the detector and is where the timing pulse will be measured.

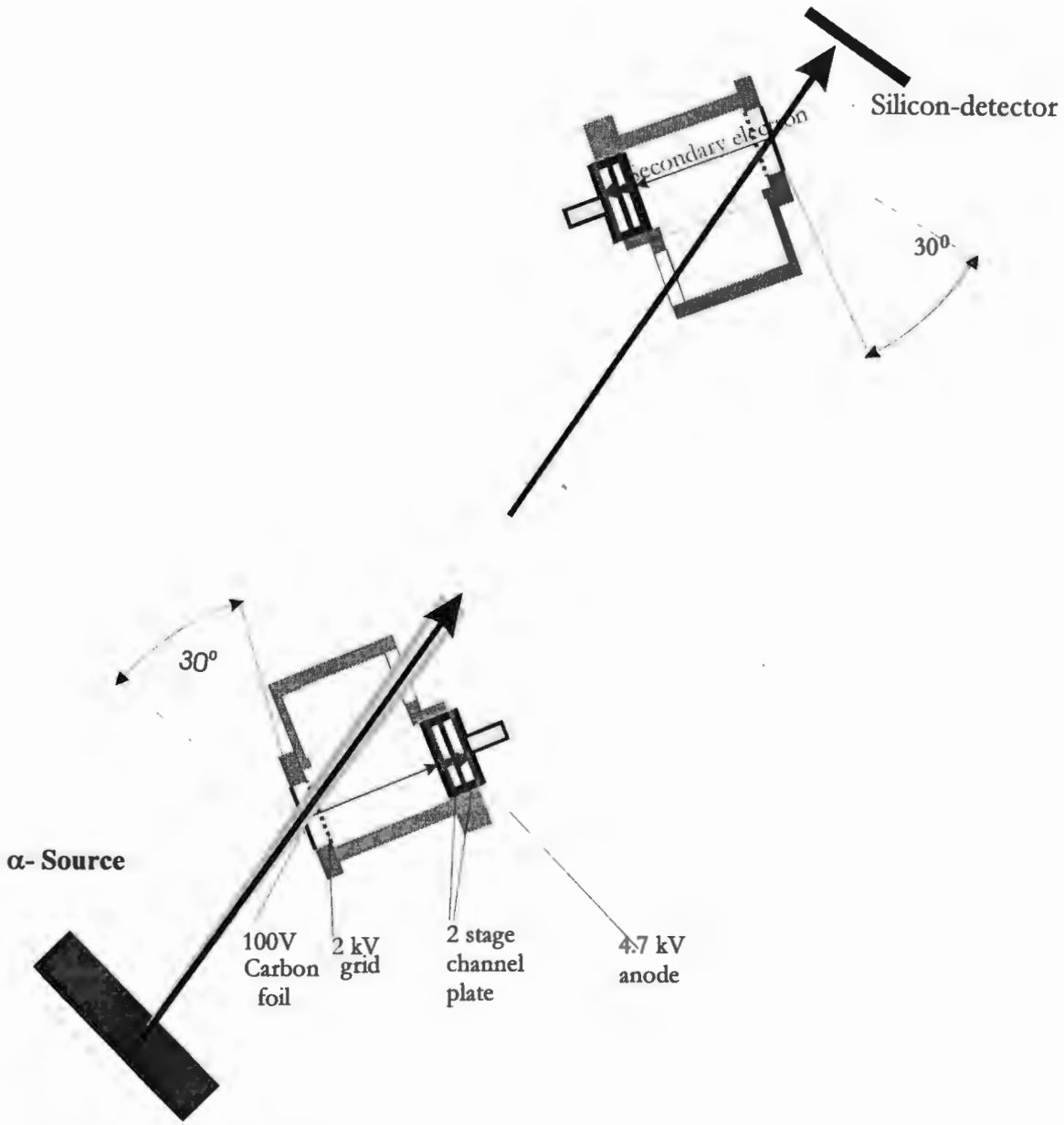

Fig 4.2 Schematic representation of the setup used to test the time of flight measurement with an alpha source.

The detectors were assembled and mounted in the vacuum chamber. An Am-241 source producing alpha particles of 5.4 MeV energy was used in the testing of the detectors. The alpha particles from the source placed 5 cm away from the first detector, strike the thin carbon foil (11μg/cm^2), which emits secondary electrons on alpha bombardment. The carbon foil sits at +100V relative to ground so that positive stray ions will be deflected and not enter the system. These emitted secondary electrons are accelerated by an electric field created by the acceleration grid. The electrons enter the first MCP and are amplified there. Acceleration into the second MCP guarantees additional gain. The electrons are accelerated from the output of the second MCPs to the anode. There is a capacitor between the anode and the output of the detector, which enable the detector to give timing pulses. A second timing detector is placed about 0.46m away from the first foil, which then gives the second timing pulse.

The applied voltage across the MCPs to get optimum operation is 1000V, but to extend the lifetime of the MCPs the detectors were powered with a voltage (see section 4.5) that is just sufficient to provide a usable signal and are discussed in section 3.2.1. The surface barrier detector was placed directly after the second carbon foil. The signal from the silicon surface barrier was taken to the preamplifier and then to the oscilloscope. The timing signals from the timing detectors were taken to the preamplifier, then a fast discriminator and were then taken to the oscilloscope. The fast discriminator was used to check whether the signal from the preamplifier exceeded the discriminator level giving a signal that could be used for coincidence control. The discriminator level had to be adjusted considerably higher than the noise level, thus when observing the input and output of the discriminator it was found that some smaller amplitude pulses from the detector were not discriminated. The necessity for setting the discriminator level that high still has to be investigated.

4.3 Start-up procedure for the MCPs

The detectors were mounted in the vacuum chamber and pumped down to a pressure of 5.8×10^{-7} mbar. The system was kept at this vacuum for more than 15 hours. The start-up procedure in Table 4.1 was followed to bake the MCPs. The voltage across the MCPs was increased in steps of 100V every 2 minutes until 500V. After waiting for 5 minutes the voltage across the MCPs was increased in steps of 50V every 5 minutes until a voltage of 800V. After 10 minutes it was further increased by 50V every 10 minutes until a potential of 1000V was reached. A 10-minute delay was made before the measurements were started.

Time (minutes)	$V_{power\ supply}$ (V)	$V_{across\ MCP}$ (V)
0	470	100
2	940	200
4	1410	300
6	1880	400
8	2350	500
13	2585	550
18	2820	600
23	3055	650
28	3525	700
33	3760	750
43	3995	850
53	4230	900
63	4465	950
73	4700	1000

Table 4.1. Showing the steps that were taken when baking the MCPs. The first column showing the time variation, the second column showing the voltages on the power supply and the last column showing the voltages across the MCPs.

4.4 Results and discussion

When testing the detectors with and without the alphas, it was observed that there was a difference between the pulses rate observed on the first timing detector. The difference between pulses on the second timing detector with the source on and off was not detectable due to the large distance between the source and the second detector, i.e. the solid angle was small and that meant that the pulses from the source were very low compared to the dark counts.

The dark counts were high causing low detection efficiency (could not be determined yet) of the system. The other observation that still needs to be investigated is that signals are observed on the silicon surface barrier detector but no corresponding signals on the timing detectors are seen and sometimes there are no signals observed on the silicon surface barrier whereas there are signals observed on the timing detectors. The two time signals could not be measured in coincidence because of the constraints that were experienced. A dual 5 kV power supply was used, however when both detectors were tested at the same time it was found that one channel was faulty. No replacement supply could be found in time. The timing signal from the silicon surface barrier was used as a reference and measurements on the timing detectors were made one after the other. For the signals to be measured in coincidence a dual power supply is necessary.

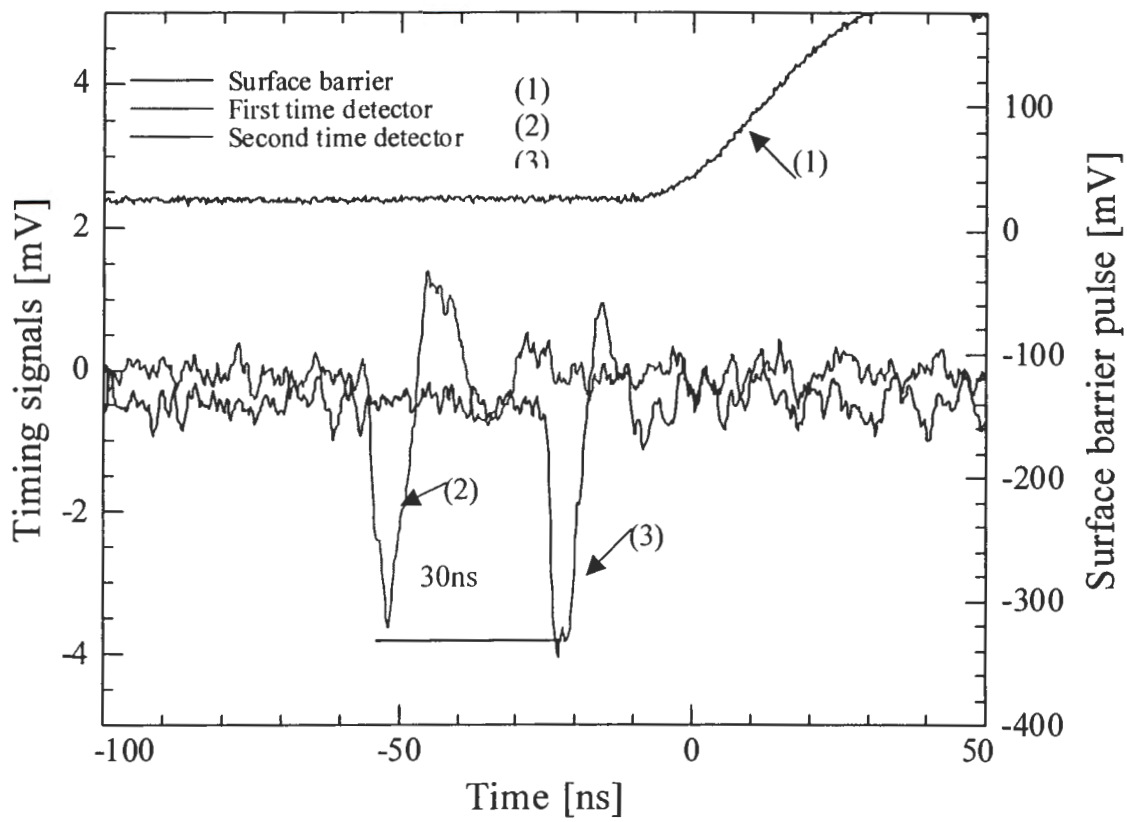

Fig.4.3 A plot of voltage (mV) versus time (ns). There are two vertical scales, one on the left is the scale for the timing signals from the two timing detectors, with one showing a pulse at about –50 ns and another at about –20 ns. The scale on the right is for the surface barrier pulses.

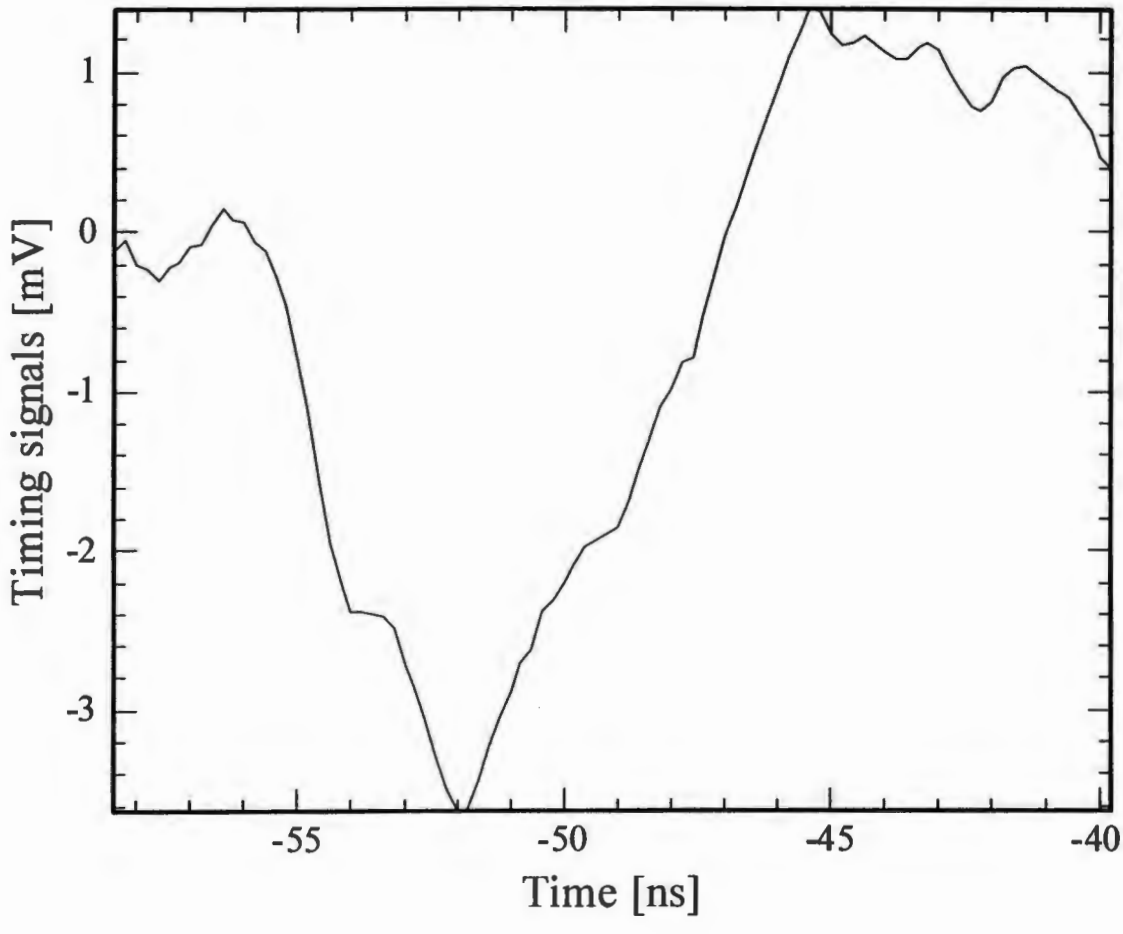

Fig 4.4. Showing the pulse from the first timing detector used to calculate the pulse width, which was found to be about 6ns. The rise time calculated at 10 and 90% is about 3 ns.

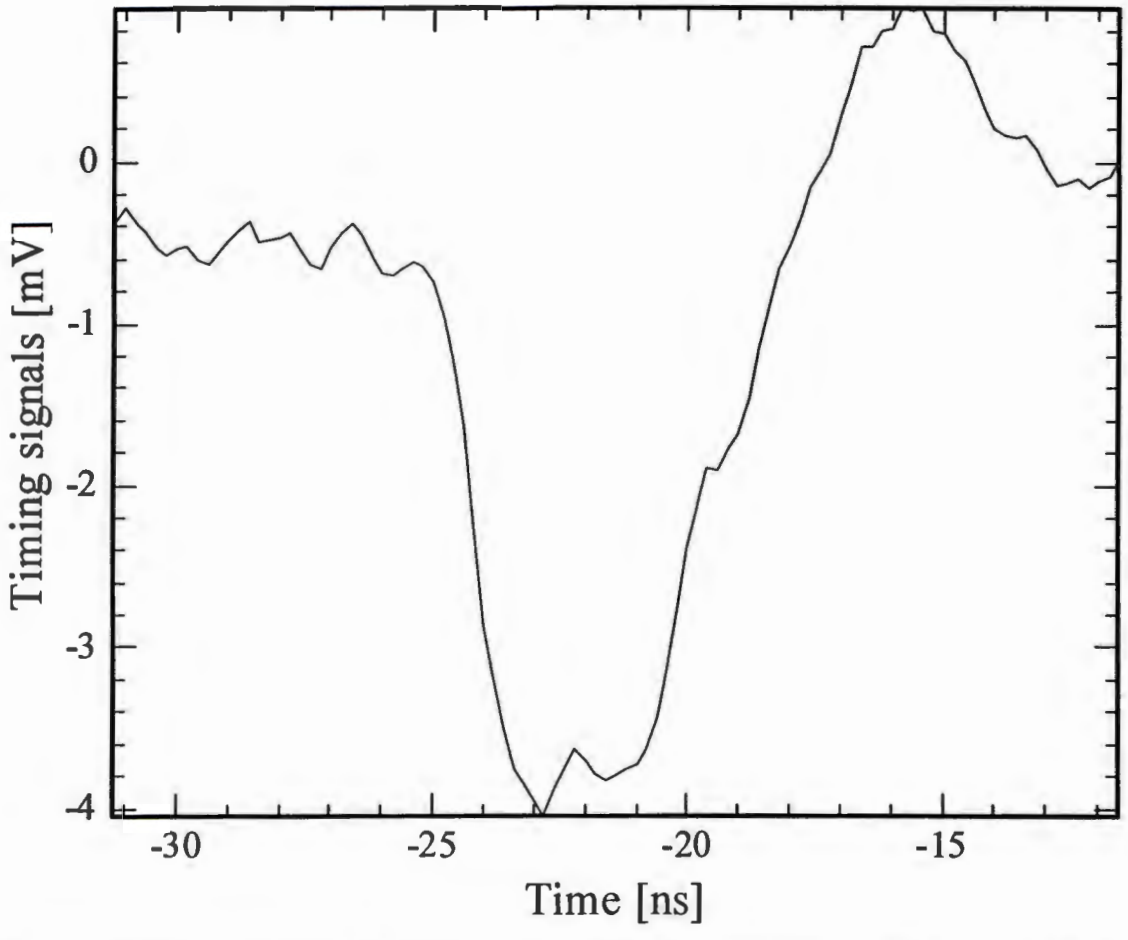

Fig 4.5. Showing the pulse from the second timing detector used to calculate the pulse width, which was found to be about 5ns. The rise time calculated at 10 and 90% is about 1 ns.

The plot in Fig.4.3 shows the results of the test done on the system using the alpha source to generate electrons on the carbon foils and the energy signals generated from the surface barrier detector. The top trace (surface barrier) was used as a reference for the two timing signals by triggering at a specified level on the silicon surface barrier signal. This was observed at the applied voltage of 3905V on the power supply, which translates to about 840V across the MCPs. This voltage was sufficient to give usable signals on the two timing detectors. The time difference between the two timing pulses is 30ns, which agrees quite well with the calculated value of 28.4 ns considering inaccuracies in the triggering levels of the silicon surface barrier.

In this test the time detectors were powered one at a time and measured with reference to the silicon surface barrier detector signals and then the time difference between the two timing signal was measured to be 30ns. The pulse width of about 6ns was obtained from the first detector (Fig 4.4) and the pulse width of about 5ns from the second detector. The detection efficiency of the detectors could not be established since; there were too many dark counts. It would be good to perform coincidence measurement on the system to able to accurately determine the time of flight of the particles in coincident with the pulses on the surface barrier detector.

There were on average 20 counts per second on the surface barrier and about 2000 counts per seconds on the first time detector. These measurements were made at vacuum of 5.8×10^{-7} mbar.

CHAPTER 5

5 Summary and future work

5.1 Summary

The aim of this study was to contribute to the implementation of ERD as a tool to be used in the analysis of elastically recoiled ions using energetic heavy ions from the Second Single Pole injector Cyclotron. As part of the overall build up to introducing ERD using TOF-E detection system, the focus of this study was (1) to construct the time of flight detector and (2) to demonstrate that useful timing signals can be detected.

The TOF-E detector was described and the design considerations are also presented. The detectors were tested both without and with the MCPs mounted. This was done so that damage to the MCPs could be minimized. Systematic tests were made following a range of modifications to the design of the detectors. The detectors were tested using an alpha source of energy 5.4 MeV. A start up procedure for the detectors was outlined.The measured timing signals from the timing detectors gave a time of flight of 30 ns for the alphas, which was comparable to the calculated value of 28.4 ns. The results showed that the implementation of ERD using TOF-E at SPC2 was promising.

5.2 Future Work

Although usable timing signals were obtained from the tests, there are many dark counts and further investigations into reducing the dark counts is recommended. The fast discriminator was used to check whether the signals from the preamplifier exceeded the discriminator level giving a signal that could be used for coincidence control. The discriminator level had to be adjusted considerably higher than the noise level, thus when observing the input and output of the discriminator it was found that some smaller amplitude pulses from the timing detectors were not discriminated. The necessity for setting the discriminator level that high still has to be investigated.

When testing the detectors with and without the alphas, it was observed that there was a difference between the pulses observed on the first timing detector. The difference between the pulses on the second timing detector with the source on and off was not detectable due to the large distance between the source and the second timing detector is small. The possibility of increasing the solid angle of detection of the second timing detector should be investigated and that means increasing the size of the silicon surface barrier detector. At this stage the silicon detector will be a strip detector, which is position sensitive to allow for the correction of the kinematic shift.

A dual 5 kV power supply was used, however when both detectors were tested at the same time it was found that one channel was faulty. No replacement supply could be found in time and coincidence measurements of the two timing detectors could not be performed, instead the timing signals from the silicon surface barrier detector were used as a reference and the measurements on the timing detectors were made one after the other. For the signals to be measured in coincidence, a dual power supply is necessary.

Refferences

[Ass 96] W. Assmass, J. A. Davies, G. Dollinger, J. S. Forster, H. Huber, Th. Reichelt, R. Siegele, 'ERDA with very heavy ion beams' Nucl. Instr. And Meth. B 118 (1996) 242.

[Ber 98] A. Bergmaier, G. Dollinger, C. M. Frey, 'A compact ΔE-E_{res} detector for elastic recoil detection with high sensitivity' Nucl. Instr. And Meth. B 136-138 (1998) 638.

[Bur] Burle Industries, INC. 'STORAGE, HANDLING and OPERATION of MICROCHANNEL PLATES' www.burle.com/dettechbrief.html

[Boh 98] W. Bohne, J. Röhrich, G. Röschert, 'The Berlin time-of-flight ERDA setup' Nucl. Instr. And Meth. B 136-138 (1998) 633.

[Dol 98] G. Dollinger, S. Karsch, O. Ambacher, H. Angerer, A. Bergmaier, O. Schmelmer, M. Stutzmann, Mat. Res. Soc. Symp. Proc. 482 (1998).

[Dol 92] G. Dollinger,T. Faestermann, P. Maie-Komor, 'High resolution depth profiling of light elements' Nucl. Instr. And Meth. B 64 (1992) 422.

[Dol 96] G. Dollinger, M. Bouloudnine, A. Bergmaier, T. Faestermann, C. M. Frey, ' Limits in elastic recoil detection analysis with heavy ions' Nucl. Instr. And Meth. B 118 (1996) 291.

[Dol 01] Private communication with Guenther Dollinger (Technical University of Munich) May 2001

[Gro 83] R. Groleau, S.C. Gujrathi and J.P. Martin, 'Time-of-flight system for profiling recoiled light elements' Nucl. Instr. And Meth. 218 (1983) 11.

[Grö 92] R. Grötzschel, E. Hentschel, R. Klabes, U. Kreissig, C. Neelmeijer, W. Assmann, R. Behrisch, 'Elemental analysis of thin layers by elastic heavy ion scattering' Nucl. Instr. And Meth. B 63 (1992) 77.

[Guj 87] S. C. Gujrathi, P. Aubry, L. Lemey, J. P. Martin, 'Nondestructive surface analysis by nuclear scattering techniques' Can. J. Phys. 65 (1987) 950.

[Hab 92] F.H.P.M. Habraken, 'Light element depth profiling using elastic recoil detection' Nucl. Instr. And Meth. B 68 (1992) 181.

[Hon 97A] Wan. Hong, Shinjuro Hayakawa, Kuniko Maeda, Shigekazu Fukuda, Minoru Yanokura, Michi Aratani, Kazuie Kimura, Yohichi Gohshi and Isao Tanihata, 'Improvement in the Detection Limits of Elastic Recoil Detection Analysis (ERDA) using a Time of Flight Detection' Jpn. J. Appl. Phys. Vol. 36 (1997) L 952.

[Hon 97B] W. Hong, S. Hayakawa, K Maeda, S Fukuda, M. Yanokura, M. Aratani, K. Kimura, Y. Gohshi, I. Tanihata, 'Development of a high mass-resolution TOF-ERDA system for a wide mass range' Nucl. Instr. And Meth. B 124 (1997) 95.

[Hon 99] Wan Hong, Shinjiro Hayakawa, Kuniko Maeda, Shigekazu Fukuda, Yohichi Gohshi, 'Light element analysis in steel by high energy heavy-ion time of flight elastic recoil detection analysis' Spectrochimica Acta Part B 54 (1999) 151.

[Kas 94] B. Kassühlke, 'Ein Elektron Flugzeitspektrometer für Oberflächenuntersuchungen: Konzeption, Aufbau und erste Anwendungen', diploma thesis, Technical University of Munich (TUM) 1994.

[Kol 93] A.Kolitsch, E. Hentschel and E. Richter, 'Depth profiles of C, N and O on carbon coated steel surfaces made by IBAD' Nucl. Instr. And Meth. B 80/81 (1993) 258.

[LÉc 76] J. LÈcuyer, C. Brassard, C. Cardinal, J. Chabbal, L. Deschěnes, J. P. Labri,B. Terreault, J. g. Martel und R. St. –Jacques, J. Appl. Phys. 47 (1976) 381.

[Lie 97] V.Kh. Liechtenstein, T. M. Ivkova, E. D. Olshanski, I. Feigenbaum, R. DiNardo, M. Döbeli, 'Preparation and evaluation of thin diamond- like carbon foils for heavy ion tandem accelerators and time-of-flight spectrometers' Nucl. Instr. And Meth. A 397 (1997) 140.

[Maa 98] Jos Maas, PhD thesis, Technical University of Eindhoven, 'Elastic Recoil Detection Analysis with α-particles' (1998)

[Mar 94] J. W. Martin, D. D. Cohen, N. Dytlewski, D. B. Garton, H. J. Whitlow, G. J. Russell, 'Materials characterization using heavy ion elastic recoil time of flight spectrometry' Nucl. Instr. And Meth. B 94 (1994) 277.

[Phi] Phillips Microchannel Plates (Bio-Teknik) www.redivo@iafrica.com

[Rop] Roperscientific technical notes (Introduction to image intensifiers for scientific imaging), www.roperscientific.com/library-technotes.shtml.

[Sto 89] J.P. Stoquert, G. Guillaume, M. Hage-Ali, J. J. Grob, C. Ganter, P. Siffert, 'Determination of concentration profiles by elastic recoil detection with a ΔE-E gas telescope and high energy incident heavy ions' Nucl. Instr. And Meth. B 44 (1989) 189.

[Tir 96] Jorge Tirira, Yves Serruys and Patrick Trocellier, 'Forward Recoil Spectrometry (Applications to Hydrogen Determination in Solids)' (1996)

[Tim 98] H. Timmers, R.G. Elliman, G.R. Palmer, T. R. Ophel, D. J. Ó Connor, 'The development of a facility for a heavy-ion elastic recoilm detection analysis at the Australian National University' Nucl. Instr. And Meth B 136-138 (1998) 611.

[Zha 99] Yanwen Zhang, Harry J. Whitlow, Thomas Winzell, Ian F. Bubb, Timo Sajavaara, Kai Arstilla, Juhani Keinonen, 'Detection efficiency of time-of-flight energy elastic recoil analysis systems' Nucl. Instr. And Meth. B 149 (1999) 477